

Unveiling the Landau Levels Structure of Graphene Nanoribbons

Rebeca Ribeiro¹, Jean-Marie Poumirol¹, Alessandro Cresti², Walter Escoffier¹,
Michel Goiran¹, Jean-Marc Broto¹, Stephan Roche^{3,4}, and Bertrand Raquet¹

¹Laboratoire National des Champs Magnétiques Intenses, INSA UPS CNRS,
UPR 3228, Université de Toulouse, 143 av. de Rangueil, 31400 Toulouse, France

²IMEP-LAHC (UMR CNRS/INPG/UJF 5130), Grenoble INP Minatéc,
3 Parvis Louis Néel, BP 257, F-38016 Grenoble, France

³CIN2 (ICN-CSIC) and Universitat Autònoma de Barcelona, Catalan Institute of Nanotechnology,
Campus de la UAB, 08193 Bellaterra (Barcelona), Spain and

⁴ICREA, Institutio Catalana de Recerca i Estudis Avançats, 08010 Barcelona, Spain
(Dated: January 12, 2013)

Magnetotransport measurements are performed in ultraclean (lithographically patterned) graphene nanoribbons down to 70 nm. At high magnetic fields, a fragmentation of the electronic spectrum into a Landau levels pattern with unusual features is unveiled. The singular Landau spectrum reveals large magneto-oscillations of the Fermi energy and valley degeneracy lifting. Quantum simulations suggest some disorder threshold at the origin of mixing between opposite chiral magnetic edge states and disappearance of quantum Hall effect.

PACS numbers: 72.80.Vp, 75.47.-m, 73.22.Pr

Introduction.— To benefit from the unusual transport properties of graphene (massless Dirac fermions physics) [1, 2], and engineer novel building blocks for future carbon-based nanoelectronics [3], the fabrication of clean materials has become a central issue. Of great concern is the design of graphene nanoribbons (GNRs) with lateral sizes in the order of a few to tens of nanometers, which allow some gap engineering [4]. The transverse confinement leads to 1D electronic sub-bands profiles whose details depend on the width and the edge geometry of the ribbons [5].

In presence of a strong perpendicular magnetic field, anomalous quantum Hall effect develops in two-dimensional graphene with unique properties widely discussed in the literature [6]. The electronic spectrum is theoretically predicted to evolve into magneto-electronic sub-bands resulting from a competition between magnetic and electronic confinement [2, 5]. This is partly unveiled by anomalous Shubnikov-de Haas oscillations when the Landau diameter becomes larger than the ribbon's width [7]. However, it is puzzling to note the lack of experimental evidence of Hall quantization in nanoribbons narrower than 200 nm [8–11]. Recent magnetotransport experiments in chemically derived narrow GNRs reported some signatures of chiral magnetic edge states revealed by a large positive magnetoconductance [10]. Positive magnetoconductance is also observed in lithographic nanoribbons [9, 11], but in all these experiments, the conductance is far from being quantized, and transport remains strongly diffusive, thus jeopardizing a convincing observation of the underlying Landau levels. Several sources of disorder are suspected to crosslink chiral edge currents for the narrowest ribbons, thus preventing quantum Hall effect from developing [12]. Additionally, for clean GNRs, recent theoretical calculations suggest a strong impact of electron-electron interactions on the band structure

leading to the suppression of the conductance quantization [13]. A detailed characterization of Landau levels in GNRs thus remains to be accomplished.

In this Letter, we report two-terminal quantum Hall resistance measurements on GNR devices. The oscillatory behavior of the magnetoresistance (MR) evidences a clear signature of magneto-electronic subbands. The onset of a singular graphene-like Landau spectrum reveals a large pinning of the Fermi energy along with a valley degeneracy lifting. To rationalize those features, we simulate the spatial extension of the corresponding magnetic edge states and their distribution in presence of disorder.

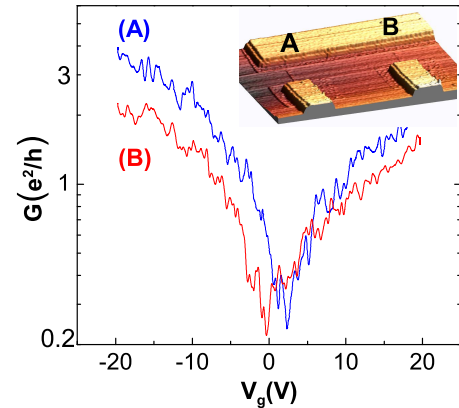


FIG. 1: (color online) Experimental $G(V_g)$ curves measured at 4.2K on two GNR devices of width 100 and 70nm (sample A and B). Inset : the AFM image of the devices.

Graphene devices are made by mechanical exfoliation of graphite onto $n^{++}\text{Si}/\text{SiO}_2(300\text{nm})$ substrates. Electrodes are defined by e-beam lithography followed by

thermal evaporation of Ti(1nm)/Pd(10nm)/Au(40nm). Next, the graphene flakes are patterned into ribbons by oxygen plasma etching, using PMMA as an etching mask. A set of connected GNRs are prepared with width (W) ranging from 60 to 100nm and length (L) from 350 to 800nm. In the following, we present extended results on two devices (inset Fig.1), sample A ($L = 350$ nm, $W = 100$ nm) and B ($L = 750$ nm, $W = 70$ nm), having the hallmarks of the overall samples.

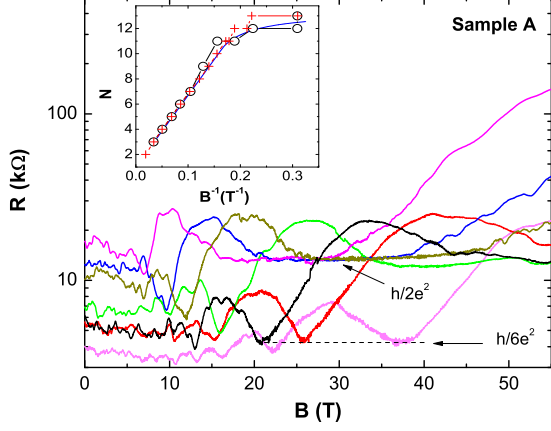


FIG. 2: (color online) Two-probe perpendicular magnetoresistance measured at 4.2K on sample A, for selected V_g from -10V (cyan) to -40V (light magenta), by step of 5V. The inset shows anomalous $1/B$ Shubnikov-de Haas oscillations with circle marks indicating the Landau index N as a function of the $1/B_i$ locations deduced from the MR curve at -40V. The red crosses are the $N_i(1/B_i)$ simulated data from the band structure (Fig. 4a, inset). The blue curve is the calculated $N(1/B_i)$ from [14].

After standard thermal annealing treatment in vacuum to desorb contaminants, the measured $G(V_g)$ at 4.2K (Fig. 1) exhibits a minimum at the charge neutrality point corresponding to a back-gate potential $V_g = V_{\text{CNP}}$, close to zero, 2.5V and -0.5V for samples A and B, respectively, thus pinpointing a negligible residual doping. From a numerical calculation of the electrostatic coupling between the ribbons and the back-gate (available at <http://www.fastfieldsolvers.com>), the carrier density is estimated as $n(\text{m}^{-2}) \approx 1.5 \times 10^{15} \times (V_g(\text{V}) - V_{\text{CNP}})$ while the Fermi energy scales as $E_F(\text{meV}) \approx 40 \times \sqrt{(V_g(\text{V}) - V_{\text{CNP}})}$. Assuming a negligible contribution of quantum interferences, we estimate the electronic mean free path, $l_m(V_g)$, from the $G(V_g)$ curves [14]. At $V_g = -20$ V, we infer $l_m \approx 50 - 120$ nm (80-120nm) for sample A(B). In both cases, $l_m \sim W$ and $L/l_m \approx 2 - 7$, this indicates that the transport regime is close to a quasi-ballistic regime. The good quality of the samples is also confirmed by the estimated large field effect mobility at 4.2K $\mu_{\text{A(B)}} \approx 1200(3500)\text{cm}^2/(\text{Vs})$, and by the Fabry-Perot conductance modulations observed at 2K [14].

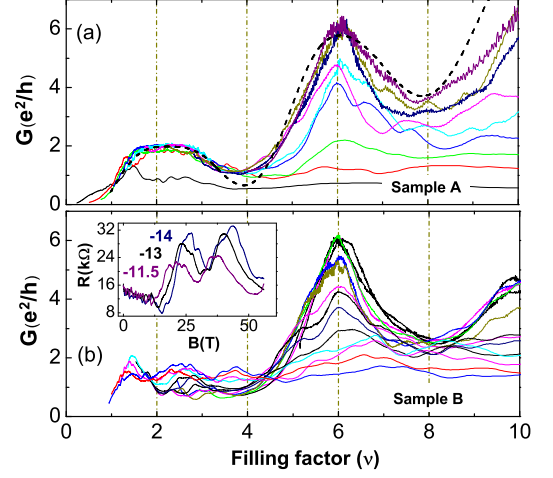


FIG. 3: (color online) (a) Experimental magnetoconductance of sample A versus the filling factor deduced from the MR curves at selected V_g , from -40V (top) to 0V (bottom), by step of 5V. The dashed line is the simulated $G(\nu)$. (b) Magnetoconductance of sample B versus the filling factor at different V_g from -50V (top) to 0V (bottom), by step of 5V. Inset: the singular MR curves exhibiting a double resistance peak when E_F crosses the $N = 2$ Landau level.

Under a perpendicular magnetic field, the two-terminal resistance shows a non-trivial sample-shape dependent profile. It reveals fingerprints of both the quantized Hall resistance for incompressible charge carriers densities (i.e. for filling factors $\nu(n_e h/eB) = 4(n + 1/2)$) and the longitudinal resistance for intermediate filling factors [15]. Accordingly, for elongated ribbons, the resistance peaks pinpoint the depopulation onset of the highest occupied Landau subband of index N . Figure 2 shows the two-probe MR up to 55T at various V_g for sample A. An oscillatory behavior of the resistance along with quantized minima ($h/6e^2$) and resistance plateaus ($h/2e^2$) are clearly visible. The MR plot as a function of the inverse magnetic field shows the expected $1/B$ Shubnikov-de Haas oscillations of the resistance peaks for a 2D electron gas [14].

However, a strong departure from the $1/B$ periodicity is observed for larger N (inset, Fig. 2 circle marks). This is a convincing signature of the electronic confinement that starts to overcome the magnetic one when the cyclotron radius becomes larger than $W/2$. The linearity and its deviation above $N \approx 9$ are well reproduced by the calculation of the number of occupied subbands $N = N(1/B_i)$ in the frame of semiclassical Bohr-Sommerfeld quantization rule with an hard-wall confinement (blue line) [14].

Figure 3 shows the conductance profiles of the two GNRs as a function of the filling factor. The curves are deduced from the MR experiments, i.e. a constant charge density along with a pulse field sweep, meaning an increase of the Landau energy broadening versus ν . For

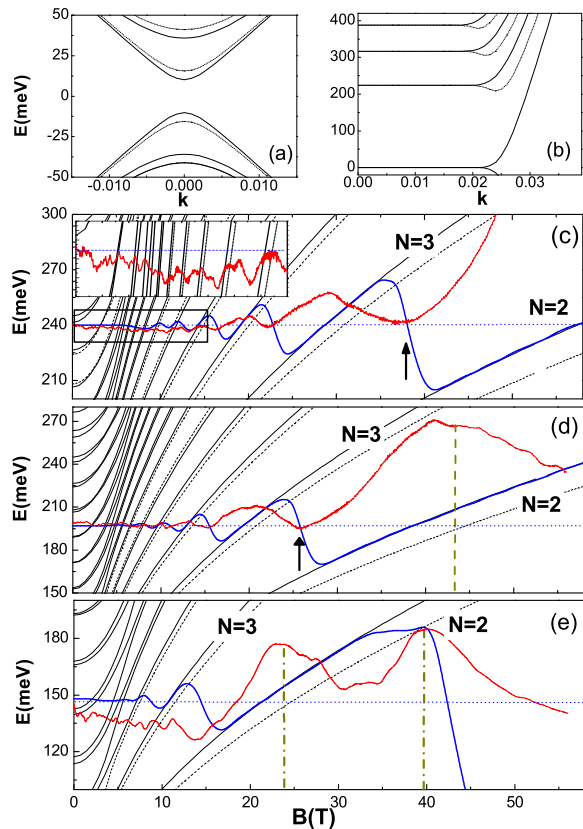


FIG. 4: (color online) (a) and (b) Band structure of a 70nm-wide aGNR around the CNP at 0 and 50T, respectively. (c-e) Simulated magneto-electronic subbands versus magnetic field for the 100nm-wide aGNR (c) and 70nm-wide aGNR (d,e) directly compared to quantum oscillations at selected E_F . Black lines hold for the edge subbands at zero- k . The dashed black lines correspond to the valley degeneracy lifting at nonzero k . In red are plotted the MR curves in arbitrary unit and in blue, the related Fermi energy. Dark yellow vertical lines indicate the resistance peaks shifted to higher magnetic field due to the Fermi energy pinning at low N .

sample A (Fig.2a), a clear $2G_0$ Hall conductance plateau is observed at $\nu = 2$, providing direct evidence of a single layer graphene. For larger incompressible charge densities, at $\nu = 6, 10, \dots$, only maxima of conductance develop instead of the expected $(6, 10, \dots)G_0$ plateaus. This overall behavior is consistently described in the context of the conformal invariance of the conductance, where the distortion of the plateau is driven by the device aspect ratio $\xi = L/W$. Following the theory developed in [15], we reasonably well simulate our data for $\xi_{fit} = 4.1$ (to be compared to $\xi_{exp} = 3.5$) and a broadening of $\Delta\nu \approx 0.84$ and 1.05 around $\nu = 2$ and 6 , respectively (Fig.3a, dashed line). The larger broadening at higher filling factor is therefore responsible for the shrinkage of the $6G_0$ quantized state.

Despite such agreement, several intriguing experimental features demand further considerations : (i) The re-

sistance peaks preceding the $h/2e^2$ plateau on sample A (i.e. corresponding to the crossing of the $N = 3$ Landau level) appear drastically enlarged for the MR curves at larger V_g (Fig.2). (ii) Surprisingly, the Hall conductance of sample B, which is 30% narrower, does not present a well-defined $2G_0$ plateau even though the $6G_0$ quantization at $\nu = 6$ is preserved (Fig.3b). The suppression of the $2G_0$ conductance plateau goes along with a well-marked splitting and broadening of the resistance peak that develops before the expected plateau (Fig.3b-inset). (iii) Both samples exhibit a gradual suppression of the $6G_0$ conductance at $\nu=6$ as V_g decreases (Fig.3a and b).

For a deeper understanding of the MR curves and the related Landau levels pattern, we now consider the magnetic field dependent band structure of two armchair ribbons (aGNRs) of width $W \approx 100$ and $W \approx 70$ nm. Due to the rather large width of the ribbons, the following discussion does not depend on the exact number of dimer lines that compose the ribbons. Figures 4(a,b) show the band structure of the narrowest aGNR around the CNP at $B=0$ and 50T, respectively. Note that the valley degeneracy of the two-dimensional graphene is lifted as a consequence of the ribbon boundary conditions [5]. At $B=50$ T, the bulk Landau levels are degenerated while the edge states (at large wavenumber k), split into couples of nondegenerate bands, among which one has an increasing energy while the other first decreases and then rises when approaching the edges of the Brillouin zone. The black (solid and dashed) lines of Fig. 4(c-e) indicate the minimum energy of each band as a function of the magnetic field. Above 10T, they start to scale as \sqrt{B} , thus converging to the Landau levels scaling of the 2-D graphene. Interestingly, the degeneracy breaking of edge states is enhanced at high fields. To relate the transport oscillations with the underlying band structure, we compare the intersection of the Fermi energy and the magneto-subbands spectrum with the locations of the maxima of resistance (red curve). Assuming a constant E_F (blue dashed line), a good agreement between the locations of the resistance peaks and the subband depopulation for high quantum numbers is observed at low fields (inset of Fig. 4a and corresponding red crosses in the inset of Fig. 2). However, a noticeable mismatch gradually increases below $N=3$ and reaches several Tesla for $N = 2$ in Fig. 4(d,e), marked by vertical dashed lines [14].

To shed light on this issue, we observe that, as in conventional 2D gas, the Fermi energy is not constant but varies to accommodate the carriers into the available magnetic field dependent subbands [14]. This determines large oscillations of the Fermi energy at low N (see the blue lines in Fig. 4), with an evident pinning at the Landau levels at high magnetic fields. The Fermi energy oscillations provide a clear explanation of the shape of the MR curves in the high field regime. Indeed, the inflexion point of the $E_F(B)$ curves in between two successive Landau levels well matches with the minima of

resistance (Fig. 4(c,d), marked by arrows). Besides, the widening of the resistance peaks at larger V_g and their shift to high fields are a direct consequence of a stronger Fermi energy pinning onto the lowest index Landau levels [14]. In this framework, the absence for sample B of a well-defined $2G_0$ plateau accompanying the splitting and the widening of the resistance peak also finds a natural explanation (Fig. 4e and [14]): The second maximum of resistance coincides with the changeover of E_F from the $N = 2$ Landau level (solid black line) to the second energy minimum at nonzero k (dashed black line). Note that such a signature of the valley degeneracy lifting on the MR curves requires a large enough energy splitting between the two sub-levels along with a pinning of the Fermi energy on the two states. These conditions are borne out on sample B, which has a higher mobility and allows for a sharper valley degeneracy lifting with an higher density of states at the subband edges.

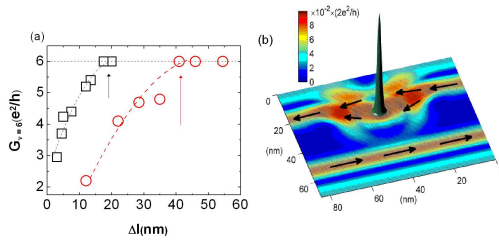


FIG. 5: (color online) (a) The measured suppression of the quantized conductance at $\nu = 6$ for sample A (red) and B (black) versus the simulated current-free bulk width Δl (nm). (b) Spatial distribution of the background spectral currents through a 70nm-wide aGNR at $\nu = 6$ ($E_F = 119$ meV and $B = 12$ T), in presence of a Gaussian potential with maximum strength $V = 1$ eV, mimicking a single charged impurity.

We finally comment on the gradual suppression of the $6G_0$ conductance at $\nu = 6$ when decreasing the back-gate voltage (Fig. 3). The deterioration of the conductance quantization at an incompressible filling factor can be related to the presence of disorder that crosslinks the chiral currents flowing at opposite edges. In [14], we simulate the spatial profile, along the transverse section of a pristine 70nm-wide aGNR, of the two counter propagating edge channels at $\nu = 6$ as a function of the magnetic field. As the magnetic field increases, the Landau states extend more and more in the bulk and the edge states are progressively pushed toward the edges. We extract the distance between the edge channels (Δl) for a given magnetic field. Figure 5a shows the measured conductance at $\nu = 6$ as a function of Δl . The conductance

starts to degrade when the corresponding edge channels in the pristine ribbon are still well separated by 40 and 15nm for the sample A and B, respectively. This is consistent with the higher degree of disorder of sample A, which is able to crosslinks the chiral currents more effectively. This behavior is very sample-dependent, since a specific disorder configuration might make the chiral currents come significantly closer, thus facilitating backscattering. Additionally, the lower V_g the more pronounced the phenomenon is, owing to a reduced screening of the impurity potential. As a matter of illustration, Fig. 5b shows the leakage of edge currents (at $N = 6$) provoked by a single charged impurity for a 70nm-wide graphene ribbon.

Conclusion.- Unusual features of Landau levels have been explored in clean graphene nanoribbons using high magnetic field transport measurements. The observed intriguing transport oscillations have been related to Fermi level pinning and valley degeneracy lifting. By means of quantum simulations, the spatial extension and robustness to disorder of chiral edge currents have been discussed.

Acknowledgements. -Sample preparations were achieved at LAAS. Part of this work is supported by EuroMagNET, contract n° 228043. S.R. acknowledges the NANOSIM-GRAPHENE Project N.° ANR-09-NANO-016-01. A.C. acknowledges the support of Fondation Nanoscience via the RTRA Disgraph project.

-
- [1] A.K. Geim and K.S. Novoselov, *Nature Materials* **6**, 183 (2007).
 - [2] A.H. Castro Neto *et al.*, *Rev. Mod. Phys.* **81**, 109 (2009).
 - [3] F. Schwierz, *Nature Nanotechnology* **5**, 487-496 (2010).
 - [4] M.Y. Han *et al.*, *Phys. Rev. Lett.* **98**, 206805 (2007).
 - [5] K. Wakabayashi *et al.*, *Phys. Rev. B* **59**, 8271 (1999); K. Wakabayashi, *Phys. Rev. B* **64**, 125428 (2001); A. Cresti *et al.*, *Nano Res.* **1**, 361 (2008).
 - [6] K.S. Novoselov *et al.*, *Nature* **438**, 197 (2005); Y.B Zhang *et al.*, *Nature* **438**, 201 (2005); K. S. Novoselov *et al.*, *Science* **315**, 1379 (2007).
 - [7] N.M.R. Peres *et al.*, *Phys. Rev. B* **73**, 241403(R) (2006); C. Berger *et al.*, *Science* **312**, 1191 (2006).
 - [8] F. Molitor *et al.*, *Phys. Rev. B* **79**, 075426 (2009).
 - [9] J.B. Oostinga *et al.*, *Phys. Rev. B* **81**, 193408 (2010).
 - [10] J. Poumirol *et al.*, *Phys. Rev. B* **82**, 041413(R) (2010).
 - [11] J. Bai *et al.*, *Nature Nanotechnology* **5**, 655-659 (2010).
 - [12] I. Romanovsky, C. Yannouleas and U. Landman, *Phys. Rev. B* **83**, 045421 (2011); E. Prada, P. San-Jose and L. Brey, *Phys. Rev. Lett.* **105**, 106802 (2010); C. Ritter, S. S. Makler and A. Latgé, *Phys. Rev. B* **77**, 195443 (2008).
 - [13] A. A. Shylau *et al.*, *Phys. Rev. B* **82**, 121410(R) (2010).
 - [14] See EPAPS Documents for supplementary material.
 - [15] J.R. Williams *et al.*, *Phys. Rev. B* **80**, 045408 (2009); D.A. Abanin and L. S. Levitov, *Phys. Rev. B* **78**, 035416 (2008).